

New Insight into Dynamic Mechanical Relaxation in N-butyl-N-(2-nitroxy-ethyl) Nitramine Plasticized Nitrocellulose through Molecular Dynamic Simulations

Xiaofei Qi

Xi'an Modern Chemistry Research Institute

ning yan (✉ yanning_204@163.com)

Xi'an Modern Chemistry Research Institute <https://orcid.org/0000-0002-4126-8738>

Hongyan Li

Xi'an Modern Chemistry Research Institute

Yu Zhao

Xi'an Modern Chemistry Research Institute

Peijin Liu

Northwestern Polytechnical University

Qilong Yan

Northwestern Polytechnical University

Research Article

Keywords: Nitrocellulose, mechanical relaxation, molecular dynamic simulations

Posted Date: July 13th, 2021

DOI: <https://doi.org/10.21203/rs.3.rs-682286/v1>

License:   This work is licensed under a Creative Commons Attribution 4.0 International License.

[Read Full License](#)

Version of Record: A version of this preprint was published at Cellulose on January 30th, 2022. See the published version at <https://doi.org/10.1007/s10570-021-04374-9>.

1 New Insight into Dynamic Mechanical Relaxation in N-butyl-N-(2-nitroxy-ethyl)
2 nitramine Plasticized Nitrocellulose through Molecular Dynamic Simulations

3
4 Xiaofei Qi^{a,b}, Ning Yan^{a*}, Hongyan Li^a, Yu Zhao^a, Peijin Liu^b, Qilong Yan^{b*}

5
6 a. Xi'an Modern Chemistry Research Institute, Xi'an 710065, China

7 b. Science and Technology on Combustion, Internal Flow and Thermo-structure
8 Laboratory, Northwestern Polytechnical University, Xi'an 710072, China

9 Authors to whom correspondence should be addressed: yanning_204@163.com (Ning
10 Yan); qilongyan@nwpu.edu.cn (Qilong Yan)

11
12 **Abstract**

13 We performed dynamic mechanical analysis (DMA) on nitrocellulose (NC) plasticized
14 by an insensitive plasticizer N-butyl-N-(2-nitroxy-ethyl)nitramine (Bu-NENA).
15 NC/Bu-NENA blend shows two mechanical relaxation processes in the temperature
16 ranges of -50~-40°C and 30~40°C, and their variations with deformation frequencies
17 were studied. To explore further the effect of temperature on relaxation, the binary
18 mixture model of NC/Bu-NENA was constructed, and molecular dynamic simulations
19 were conducted. The simulated mean square displacements (MSD) show abrupt
20 increase in the temperature range of -50~-40°C and 30~40°C, which are consistent with
21 those of the two relaxation processes observed in the DMA curves. Moreover, the free
22 volume (V_{free}) and torsion energy obtained from molecular dynamic simulations exhibit
23 distinct increase at the temperature above 30°C and -50°C respectively, reflecting the
24 sudden enhancements on the mobility of polymer chain elements and the rotation of
25 molecular bonds. Furthermore, the radial distribution function (RDF) associated with
26 the intermolecular interactions reveals that the intensities of both hydrogen bond and
27 van-der-vaals forces decrease with the increase of temperature, which is responsible for
28 the decrease of storage modulus at high temperature. These computational and
29 experimental studies reveal guidance to strengthening the NC base propellants in broad
30 temperature range.

31 **Key words**

32 Nitrocellulose, mechanical relaxation, molecular dynamic simulations

33

34 Nitrocellulose (NC), an energetic binder has been widely used in the fabrication of
35 double base propellants, wherein NC serving as a major ingredient exerts great
36 influence on the physical properties of propellants. Specifically, the mechanical
37 properties of propellants at varied temperature play important role in dominating their
38 practical applications. Nevertheless, NC features uneven rigidity nature, making it very
39 difficult to uniformly mix with other ingredients, thus imposing adverse effect on the
40 mechanical properties. In general, nitroglycerin (NG) was used as plasticizer to improve
41 the processing of NC, and the influence of NG on the physical properties of NC has
42 been well investigated (Yang et al. 2017; Ma et al. 2008; Qi et al. 2019).

43 Recent works revealed that the replacement of NG with insensitive energetic
44 plasticizers has significantly reduced the friction and impact sensitivities, which
45 facilitate to improving the process security and the vulnerability of propellants
46 (Chakraborty et al. 2004; Damse et al. 2009; Yang et al. 2014; Reese et al. 2014)

47 Moreover, the employment of insensitive plasticizers can strengthen the thermal
48 stability and lower the vaporization rate compared with NG plasticizer, which
49 contributes to enhancing mass homogeneity of NC base propellants during storage
50 (Zhao et al. 2017; Wilker et al.2007; Ou et al. 2018). It is well known that the physical
51 properties of NC show strong dependence on the additives used in propellants. In the
52 reported works, the influences of solid fillers and plasticizers have been described for
53 analyzing the physical properties of NC base propellants (Sun et al. 2018; An et al. 2012;
54 Wu et al. 2020; Wang et al. 2019; Qi et al. 2020).

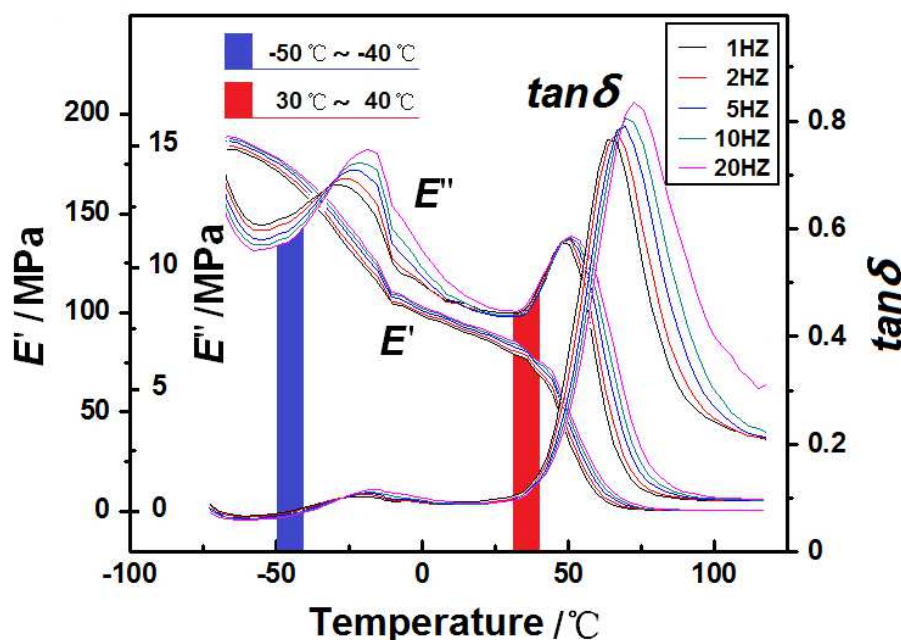
55 The static stress-strain relationship at different temperatures was depicted, which
56 offer rational explanation for the factors that affect the physical properties. In
57 comparison to static mechanical analysis, the changes in physical properties of NC can
58 be better identified in the dynamic mechanical analysis (DMA), as DMA measurements
59 possess advantages in identifying distinguishing the relaxation of polymer chains
60 associated with the storage modulus (E'), loss modulus (E''), and $\tan \delta$ (ratio of E''/E')

61 as a function of temperature (De Paula et al. 2019). The influences of plasticizers on
62 the dynamic mechanical properties of NC base propellants have been investigated,
63 revealing the existence of two principal relaxation processes at high (+40°C) and low
64 (-35°C) temperatures (Warren et al. 1988; Baker et al. 1987). Although, many
65 applications of DMA have been explored for the study of dependence of the mechanical
66 forces and energy loss on the temperature and frequency, fewer attention was paid on
67 the manner whereby the plasticizers impact the transition behavior of NC. Especially,
68 the molecular mechanism of the influence of plasticizer on the relaxation of NC is not
69 well understood. As a main factor affecting the relaxation, the interaction between NC
70 and plasticizer could be evaluated more precisely at high plasticizer content, which will
71 impose great safety issues when using sensitive plasticizers.

72 In this contribution, we replaced NG with an insensitive plasticizer N-butyl-N-(2-
73 nitroxy-ethyl)nitramine (Bu-NENA) to overcome the safety restriction, and prepared
74 NC/Bu-NENA composite with a mass ratio of 1:1. The dynamic mechanical properties
75 of NC/Bu-NENA were studied as a function of temperature, aimed to distinguish the
76 relaxations and transitions in the plasticized NC. Furthermore, molecular dynamics
77 simulations were conducted to study the role of Bu-NENA in the relaxation behavior
78 of NC, and the simulated parameters such as mean squared displacement, free volume,
79 and potential energy were correlated with the motion of molecular chains and chemical
80 bonds. These experimental and simulative studies enable better explanation of the
81 dependence of physical properties on the temperature, and reveal ~~great~~ potential
82 guidance to strengthening the NC propellants in broad temperature range.

83 N-butyl-N-(2-nitroxy-ethyl) nitramine (Bu-NENA) was purchased from Haohua
84 Chemical Group, Co., Ltd., China. Nitrocellulose (NC) was purchased from Sichuan
85 Nitrocell Co., Ltd., China. All the reagents were used without further purification unless
86 otherwise specified. The nitrocellulose pellets (nitrogen content 11.9wt%) were mixed
87 with the same mass of Bu-NENA in a vertical kneading machine (HKV-II) under
88 vacuum for 30 min. Then, the mixture was solidified for 96h at 70°C, and the as-
89 prepared composite was cut into specimen with a dimension of 4mm×4 mm×12mm.
90 The dynamic mechanical analysis (DMA) was carried out on a DMA instrument

91 (Netzsch 242) in a tension model. The DMA measurements ran at the temperature
 92 ranging from -70 °C to 110°C with a heating rate of 4K · min⁻¹, and the DMA curves
 93 were collected at the deformation frequencies of 1, 2, 5, 10 and 20 Hz, respectively.



94
 95
 96

Fig.1 Dynamic mechanical curves of NC/Bu-NENA

97 Fig.1 shows the storage modulus E' , loss modulus E'' and the loss factor $\tan \delta$ of the
 98 NC/Bu-NENA composite obtained by DMA in tension mode at five different
 99 deformation frequencies. All the loss factor curves acquired at constant heating rate of
 100 4k · min show two peaks centered at low and high temperature correlating to the β and
 101 α transitions respectively. The β transition has been attributed to the motion of
 102 plasticizer molecules associated with NC side groups, whereas the designation of the α
 103 transition is less definite, which is assumed as the relaxation of the stiff NC chain rather
 104 than a transition (Warren et al. 1988; Baker et al.1987). The splitting phenomenon was
 105 not observed in the α peak, indicating that unique state exists in the glass transition
 106 process of the NC/Bu-NENA specimens.

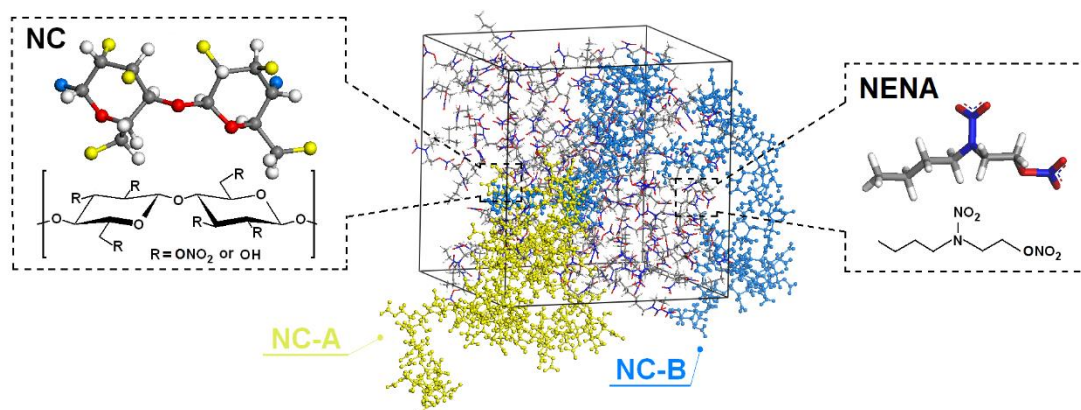
107 Dynamic mechanical properties NC/Bu-NENA show strong dependence on the
 108 relaxation of polymer chains near the glass to rubber transition temperature (T_g).
 109 Typically, increasing temperature above T_g allows to increase the free volume of
 110 polymer, and thus lead to increased molecular mobility. Oppositely, the NC/Bu-NENA

111 composite becomes hard and brittle below T_g , because of the reduced free volume at
112 low temperature. In fact, DMA has been preferentially employed to study the relaxation
113 and transition that are undetectable by DSC and TMA ([Zhang et al. 2013](#); [Saba et al.](#)
114 [2018](#); [Meng et al. 2014](#); [Bohn et al. 2015](#); [Seyidoglu et al. 2020](#)).

115 Herein, DMA was conducted at a constant heating rate and at different deformation
116 frequencies. The storage (elastic) modulus (E'), loss (viscous) modulus (E'') and loss
117 factor ($\tan\delta$) equivalent to the ratio E''/E' were recorded as a function of temperature.
118 As shown in Fig.1, the storage modulus (E') gradually decreases with the increase of
119 temperature in the case of all frequencies, implying that the energy storage per unit
120 strain was lowered at high temperature. In general, mechanical relaxation occurs in the
121 glass transition process of polymers, during which the flexibility and mobility of
122 molecular chains undergo prominently changes. The decreased storage modulus is an
123 indication of the increased mobility of NC/Bu-NENA chains at high temperature.
124 Oppositely, increasing the deformation frequency in DMA leads to an increase of the E'
125 value at the same temperature, and this is due to the strain-rate hardening effect of
126 polymer chains at high deformation frequencies ([Bohn et al. 2015](#);). The curves of loss
127 modulus versus temperature show two peaks centered at around -25°C and 50°C , which
128 are associated with the maximum energy loss arising from the internal friction and
129 molecular rearrangement processes of polymer chains.

130 Moreover, the loss modulus curves show two inflection points at the temperature of
131 -50°C and 30°C , corresponding to the onset temperatures of multiple relaxations of
132 polymer chains. At the temperature of -50°C , the side chain elements of NC start
133 moving as the imported thermal energy overcomes their energy barrier. Increasing the
134 temperature up to 30°C initiates the cooperative motion of numerous chain segments,
135 which allows large scale deformation of NC/Bu-NENA, and hence lowers the storage
136 modulus. Besides, the $\tan\delta$ curve representing ratio of E''/E' was plotted against
137 temperature, and the maximum value of $\tan\delta$ is a measure of glass transition
138 temperature. The $\tan\delta$ curves show two peaks reflecting the damping characteristics of
139 NC/Bu-NENA at low and high temperatures, respectively. In fact, the intrinsic
140 properties of polymer binders or plasticizers experience substantial change from glass

141 state to rubber state by increasing temperature, which is an indicator of the change in
 142 the molecular mobility of the polymeric networks during the glass-rubber transition.
 143 Moreover, the maximum $\tan\delta$ value and its corresponding glass transition temperature
 144 increase with the increase of frequency, which is due to the freeze of the polymer chain
 145 elements at high tensile frequency.



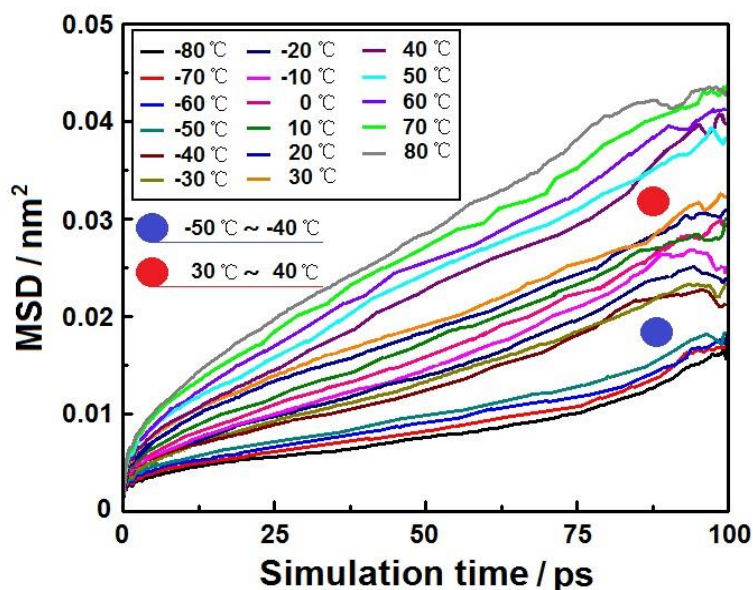
146
 147 Fig.2 Molecular structures of NC and Bu-NENA, and the simulated primitive cell of
 148 the NC/Bu-NENA blend, NC-A and NC-B represent two different molecular chains of
 149 NC in the constructed model.

150 To gain deep insights into the variation of dynamic mechanical properties from
 151 the perspective of the motion of polymer chains, and explain the effect of temperature
 152 on the mechanical relaxation process of NC/Bu-NENA at molecular level, the
 153 molecular dynamic simulations were performed to study the atomistic model of NC/Bu-
 154 NENA by means of Material Studio (Accelrys) according to our previous work (Qi et
 155 al. 2019). Given that the nitrogen content of NC is 11.9wt%, the average degree of
 156 substitution of NC is calculated to be 2.2 according to the reported equation (Jamal et
 157 al. 2020)

$$DS = \frac{1.62 \times \%N}{14 - 0.45 \times \%N}$$

158
 159 Regarding the NC/Bu-NENA blends, the molecular chains of NC are coarse grained
 160 into the model of Gaussian chains, which are constituted by numerous basic NC units.
 161 Herein, 320 and 240 basic NC units were taken in the NC-A and NC-B Gaussian chains
 162 respectively. The simulations were conducted under a COMPASS (Condensed-phase
 163 Optimized Molecular Potentials for Atomistic Simulation Studies) force field. In detail,
 164 2 molecular chains of NC were mixed with 98 molecules of Bu-NENA in the simulated

165 primitive cell as shown in Fig.2, given that the mass ratio of NC and Bu-NENA is 1:1.
 166 The NC/Bu-NENA was optimized by a 5000 step energy minimization to regulate
 167 unbalanced configurations. To achieve an equilibrium structure, a 100ps molecular
 168 dynamic simulation was performed on the system in the NPT ensemble under constant
 169 pressure with a time step of 1fs. The simulations were carried out at different
 170 temperatures of -80, -70, -60, -50, -40, -30, -20, -10, 0, 10, 20, 30, 40, 50, 60, 70 and
 171 80°C, and the simulation results including the mean-square displacement, volume
 172 distribution, potential energy and radial distribution function were obtained.



173
 174 Fig.3 Mean-squared displacements of NC/Bu-NENA.

175
 176 To probe the dynamics of Bu-NENA molecules and assess its influences on the
 177 relaxation of NC, the mean-squared displacements (MSD) of plasticizer was estimated
 178 through molecular dynamics simulations. MSD is a statistical average of the trajectory
 179 of plasticizer molecules with simulation time and can be estimated from the production
 180 stage of MD simulation, during which the drift of the center of mass of the simulation
 181 box is subtracted, and expressed by the following equation:

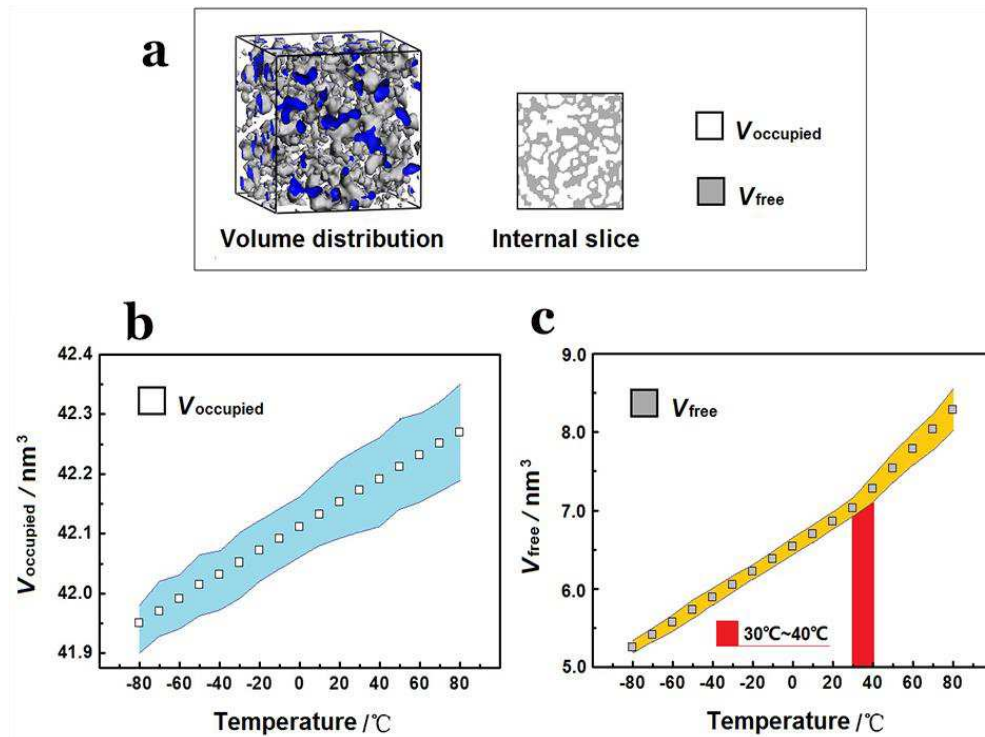
$$MSD = \left\langle |r_t - r_0|^2 \right\rangle$$

182
 183 where r_0 and r_t represent the positions of the centre of mass of plasticizer molecules at
 184 time 0 and t respectively, and the angular bracket represents the ensemble average.
 185 Typically, MSD allows to describe the diffusion of plasticizer in NC/Bu-NENA blend.

186 In brief, when the blend is frozen then MSD saturate, and the kinetic energy is too low
187 to achieve thermal diffusion. Nevertheless, if the blend is not frozen then the MSD
188 increases almost linearly with time, which allows to understand the dynamics of the
189 blend from the slope of the MSD.

190 Herein, molecular dynamic simulations were conducted to determine the MSD curves
191 versus simulation time at -80, -70, -60, -50, -40, -30, -20, -10, 0, 10, 20, 30, 40, 50, 60,
192 70 and 80 °C respectively, as shown in Fig.3. Notably, the simulations at higher
193 temperature result in larger MSD values. The MSD curves show approximately linear
194 relationship with respect to the simulation time, and the slop reflecting the mobility of
195 plasticizer molecules increases with the increase of temperature. More interestingly, the
196 slops of MSD exhibit two distinct increases in the temperature ranges from -50°C~
197 40°C and 30°C~40°C, suggesting that the molecular mobility of the plasticizer was
198 significantly enhanced, which may be due to the sudden increased free volume of NC
199 polymer in those two temperature ranges. The increased free volume facilitates to
200 promote the relaxation of NC polymer chains. The relaxation processes disclosed in the
201 MSD simulation are consistent with those revealed in DMA curves, verifying that
202 NC/Bu-NENA possesses two principle mechanical relaxations in the temperature
203 between -80 and 80°C. It should be noted that the temperature at which the mechanical
204 relaxation happens revealed in MSD is about 25°C, which is lower than the glass
205 transition temperature determined from the maximum $\tan\delta$ value, and this delay is due
206 to the viscoelastic nature of NC/Bu-NENA that leads to strain hysteresis of polymer
207 chains under the action of external force.

208



209

210

Fig.4 Volume distribution of NC/Bu-NENA at different temperatures

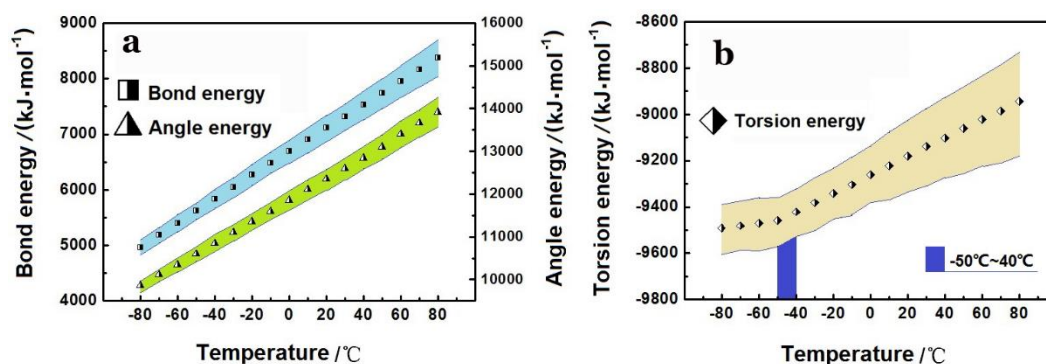
211

212 It is well established that the total volume of polymer consists of the volume occupied
 213 by polymer chains ($V_{occupied}$) and the interstitial spaces among the chains, namely free
 214 volume (V_{free}), among which V_{free} strongly affects the motion and relaxation of
 215 molecular chains. Hence, to further correlate the dynamic mechanical properties with
 216 the motion of polymer chains, the molecular dynamic simulations were conducted to
 217 study the volume distribution in the NC/Bu-NENA blend. Fig.4a shows the volume
 218 distribution of NC/Bu-NENA at different temperature, where the distribution of $V_{occupied}$
 219 and V_{free} are visualized as white and grey areas in the cubic box, and the blue area
 220 indicates the cross section of free volume.

221 Fig.4b and c show the variation of $V_{occupied}$ and V_{free} with respect to temperature. The
 222 V_{free} value exhibits substantial increase from 5.258 to 8.287 nm^3 with the temperature
 223 increasing from -80 to 80°C, whereas the $V_{occupied}$ value shows only slightly increase
 224 from 41.951 to 42.270 nm^3 , attributed to the unveiling of the overlapped volume at high
 225 temperature. It is noteworthy that the V_{free} value shows a faster increase when the
 226 temperatures are higher than 30°C. This result indicates that a critical temperature exists,
 227 at which the mobility of NC molecular chains significantly changes, resulting in an
 228 acceleration of the mechanical relaxation of the molecular chains of NC. This variation

229 of free volume is consistent with the simulation for the mean-squared displacements
 230 (MSD) in the temperature range of 30~40°C, which allows to clarifying the mechanical
 231 relaxation and transition processes occurred at high temperature revealed in DMA.
 232 Actually, the sudden change of free volume is closely related to the glass transition of
 233 NC/Bu-NENA blend. The fast increase of free volume enables cooperative motion of
 234 numerous chain segments, and allows large scale deformation, with consequence of
 235 significant reduction of modulus.

236 *Potential energy*

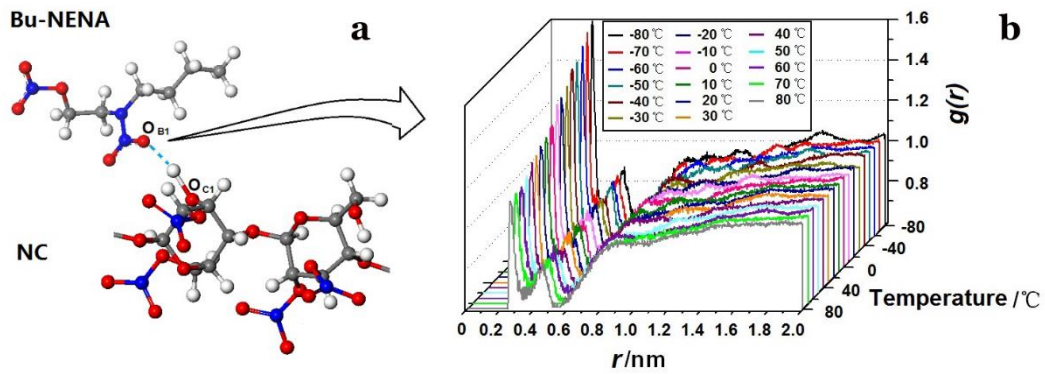


237

238 Fig.5 Potential energies of NC/Bu-NENA at different temperatures

239 In addition to free volume and mean square displacements, the potential energies
 240 consisting of intramolecular and intermolecular energies acquired from molecular
 241 dynamics simulation was adopted to study the mobility of polymer chains. Considering
 242 the arrangement of atoms in the molecular structure of NC/Bu-NENA, the potential
 243 energy consists mainly of bond energy, angle energy and torsion energy of the
 244 molecular chains. Fig.5 shows the potential energy of NC/Bu-NENA as a function of
 245 temperature. Obviously, all the potential energies increase with the increase of
 246 temperature, suggesting that the intermolecular interaction between NC and Bu-NENA
 247 was enhanced. The bond energy and angle energy exhibit almost linear increase as
 248 shown in Fig.5a, whereas the torsion energy displays two steps increase separated by
 249 the temperature region from -50 to -40°C, as highlighted in Fig.5b. This phenomenon
 250 shows a good agreement with the simulated mean square displacements at low
 251 temperature, indicating that the torsion movement in the molecular chains happened
 252 due to their shortened relaxation time in the temperature ranging from -50 to -40°C.
 253 This result can also explain the mechanical relaxation process taking place at the low

254 temperature revealed in DMA.



255

256 Fig.6 RDF curves for $O_{C1}-O_{B1}$ atom pair in the NC/Bu-NENA at different
257 temperatures.

258 To understand the effects of temperature on the dynamic mechanical properties at the
259 molecular level, the pair correlation function (PCF) was used to describe the
260 intermolecular interaction between NC and Bu-NENA. PCF allows to depict the local
261 spatial correlation of atom pairs, and enables measuring the atom density at certain
262 distance from a reference atom. The pair correlation function can be defined as

$$263 \quad g^{(2)}(r, r') = \langle v^{(2)}(r, r') \rangle / n^2$$

264 where n is the particle number density, and $v^{(2)}(r, r')$ is pair density, which is expressed
265 as:

$$266 \quad v^{(2)}(r, r') = \sum_i \sum_j \delta(r_i - r) \delta(r_j - r') \\ (i \neq j)$$

267 in which r_i and r_j is the position vector of atoms i and j respectively. The types and
268 intensities of interaction force can be judged from the peak position and peak height in
269 the PCF curves. Generally, the r values of hydrogen bond and van der waal force are in
270 the range of 0.20-0.31 nm and 0.31-0.50 nm, respectively.

271 Herein, we studied on the potential interaction forces formed between the hydroxyl
272 groups of NC and the nitrate groups of Bu-NENA. For simplicity, the oxygen atom in
273 the hydroxyl group of NC was labeled as O_{C1} , while the oxygen atom in the nitro group
274 of Bu-NENA was denoted as O_{B1} . Fig.6a illustrates the interaction between NC and Bu-
275 NENA at molecular level, and the variations of $O_{C1}-O_{B1}$ atomic force with respect to

276 temperature are shown Fig.6b. The RDF curve for the atom pair $O_{C1}-O_{B1}$ at -80°C
277 displays a peak at 0.259nm , corresponding to a $g(r)$ value of 1.606 , which indicates that
278 the type of atomic force $O_{C1}-O_{B1}$ belongs to the hydrogen bond. The second peak
279 observed at $r=0.447\text{nm}$ corresponds to the $g(r)$ value of 0.887 , and this peak is
280 associated with the van der waal forces between the oxygen functionalities in NC and
281 Bu-NENA. Notably, the intensities of both peaks in RDF curve decrease with the
282 increase of temperature, suggesting that both hydrogen bond and van der waal force
283 decrease. The decrease of intermolecular interaction enables enhancement on the
284 flexibility of NC molecular chains, which interprets the decrease of storage modulus
285 with increasing temperature.

286 In summary, NC/Bu-NENA was prepared through a conventional kneading approach.
287 DMA reveals two main relaxation processes at high and low temperatures, which
288 correlate with the movements of the molecular chains and the torsion of the molecular
289 bonds. Molecular dynamics simulations were conducted to verify the experimental
290 results. The simulated mean square displacements and free volume demonstrate abrupt
291 increase in the temperature range of $30\sim 40^{\circ}\text{C}$, which confirm the mechanical relaxation
292 and transition processes revealed in DMA. Moreover, the simulated torsion energy
293 displays significant increase in the temperature range from -50 to -40°C , which verifies
294 the torsion relaxation of molecular bonds revealed at the low temperature range of DMA
295 curves. Besides, the lower intermolecular interaction at higher temperature observed in
296 radial distribution function is the reason for the decreased storage modulus of NC/Bu-
297 NENA with increasing temperature.

298 **Acknowledgement**

299 This work is financially supported by the National Science Foundation of China
300 (21703167), and National defense basic science foundation of China (61407200204)

301

302 **Conflict of interest** The authors declare that they have no conflict of interest.

303

304 **References**

305 Yang J, Gong X, Wang G (2017) Density functional theory and molecular dynamic
306 investigations on the energetic and mechanical properties of

307 nitrocellulose/nitroglycerin/pentaerythritol diazido dinitrate composites. *Polymer*
308 *Composites* 38:192-198. <https://doi.org/10.1002/pc.23575>

309 Ma X, Zhu W, Xiao J, Xiao H (2008) Molecular dynamics study of the structure
310 and performance of simple and double bases propellants. *J Hazard Mater* 156: 201-
311 207. <https://doi.org/10.1016/j.jhazmat.2007.12.0685>

312 Qi X, Li H, Zhao Y, Yan N (2019) Comparison of the structural and physical properties
313 of nitrocellulose plasticized by N-butyl-N-(2-nitroxy-ethyl) nitramine and
314 nitroglycerin: Computational simulation and experimental studies. *J Hazard Mater*
315 362: 303-310. <https://doi.org/10.1016/j.jhazmat.2018.09.033>

316 Chakraborty T, Raha K, Omprakash B (2004) A study on gun propellants based on
317 butyl-NENA. *J Energy Mater* 22: 41-53.
318 <https://doi.org/10.1080/07370650490438293>

319 Damse R, Omprakash B, Tope B, Chakraborty T, A. Singh (2009) Study of N-
320 nbutyl-N-(2-nitroxyethyl)nitramine in RDX based gun propellant. *J Hazard Mater*
321 167: 1222-1225. <https://doi.org/10.1016/j.jhazmat.2008.12.095>.

322 Yang J, Gong X, Wang G (2014) Theoretical studies on the plasticizing effect of DIANP
323 on NC with various esterification degrees. *Comp. Mater. Sci.* 95: 129-135.
324 <https://doi.org/10.1016/j.commatsci.2014.07.024>

325 Reese D, Groven L, Son S (2014) Formulation and Characterization of a New
326 Nitroglycerin-Free Double Base Propellant. *Propellants Explos Pyrotech* 39: 205-
327 210. <https://doi.org/10.1002/prop.201300105>

328 Zhao B, Zhang T, Wang Z, Sun S, Ge Z, Luo Y (2017) Kinetics of Bu-NENA
329 evaporation from Bu-NENA/NC propellant determined by isothermal
330 thermogravimetry. *Propellants Explos Pyrotech* 42: 253-259.
331 <https://doi.org/10.1002/prop.201600054>

332 Wilker S, Gjersoe R, Stenslands P, Becher C (2007) Stability analysis of n-butyl-
333 nitrate ethylnitramine (Bu-NENA) *Cent Eur J Energy Mater* 4:59-80.

334 Ou Y, Sun Y, Guo X, Jiao Q (2018) Investigation on the thermal decomposition of
335 hydroxyl terminated polyether based polyurethanes with inert and energetic
336 plasticizers by DSC-TG-MS-FTIR. *J Anal Appl Pyrolysis* 132:94-101.

337 <https://doi.org/10.1016/j.jaap.2018.03.011>

338 Sun S, Zhang T, Zhao B, Zhang G, Li X, Luo Y (2018) Influence of
339 polytetrafluorethylene on the mechanical and safety properties of a composite
340 modified double base propellant. *Cent Eur J Energy Mater* 15:468-484.
341 [10.22211/cejem/92444](https://doi.org/10.22211/cejem/92444)

342 An, CW; Li, FS; Wang, JY; Guo, XD (2012) Surface Coating of Nitroamine Explosives
343 and Its Effects on the Performance of Composite Modified Double-Base
344 Propellants. *J Propul Power* 28: 444-448. <https://doi.org/10.2514/1.B34061>

345 Wu Z, Liu N, Zheng W, Chen J, Song X, Wang J, Cui C, Zhang D, Zhao F.
346 (2020) Application and properties of CL-20/HMX cocrystal in composite
347 modified double base propellants, *Propellants Explos Pyrotech* 45:92-100.
348 [https://doi: 10.1002/prop.201900245](https://doi.org/10.1002/prop.201900245)

349 Wang J, Yang L, Zheng W, Zhang J (2019) Study on comparative performance of CL-
350 20/RDX-based CMDB propellants. *Propellants Explos Pyrotech* 44:1175-1182.
351 <https://doi.org/10.1002/prop.201900029>

352 Qi L, Ma Z, Liang J (2020) Effect of solid additives on the rheological property
353 of nitroglycerin plasticized nitrocellulose. *Appl Rheol* 30: 14-26.
354 <https://doi.org/10.1515/arh-2020-0002>

355 De Paula A, Uliana F, Filho E, Soares K, Luz P (2019) Use of DMA-material pocket
356 to determine the glass transition temperature of nitrocellulose blends in film form
357 *Carbohydr Polym* 226:115288. <https://doi.org/10.1016/j.carbpol.2019.115288>

358 Warren R (1988) Transitions and relaxations in plasticized nitrocellulose. *Polymer* 29:
359 919-923.

360 Baker F, Privett G (1987) Dynamic mechanical studies of nitrocellulose nitroglycerine
361 mixtures polymer. 28:1121-1126. [https://doi.org/10.1016/0032-3861\(87\)90253-9](https://doi.org/10.1016/0032-3861(87)90253-9)

362 Zhang Y, Adams R, Silva L (2013) A rapid method of measuring the glass transition
363 temperature using a novel dynamic mechanical analysis method. *J Adhesion* 89:
364 785-806. <https://doi.org/10.1080/00218464.2013.763677>

365 Saba N, Jawaid M (2018) A review on thermomechanical properties of polymers and
366 fibers reinforced polymer composites. *J Ind Eng Chem* 67: 1-11.

367 <https://doi.org/10.1016/j.jiec.2018.06.018>

368 Meng F, Geng J, Besser F, Kramer M, Ott R (2014) Glass transition in a marginal glass-
369 forming alloy studied by dynamic mechanical analysis. *J Appl Phys* 116: 223505.
370 <https://doi.org/10.1063/1.4904195>

371 Seyidoglu T, Bohn M (2021) Effects of four isocyanates and four plasticizers on the
372 thermomechanical and tensile properties of hydroxylterminated polybutadiene
373 elastomers and the effect of solid particle filling. *J Appl Polym Sci.* 138: 50362.
374 <https://doi.org/10.1002/app.50362>

375 Bohn M Modelling of loss factors of elastomer binders of high explosive charges and
376 composite rocket propellants to separate binder fractions with different molecular
377 mobility used to follow ageing. Seminar on New Trends in Research of Energetic
378 Materials, Proceedings. Pt.2: April 15-17. 2015 Pardubice, Czech Republic

379 Jamal S, Roslan N, Shah N, Noor S, Ong K, Yunus W (2020) Preparation and
380 characterization of nitrocellulose from bacterial cellulose for propellant uses.
381 *Materials Today: Proceedings.* 29: 185-189.
382 <https://doi.org/10.1016/j.matpr.2020.05.540>